PCCP

PAPER

View Article Online
View Journal | View Issue

Cite this: *Phys. Chem. Chem. Phys.*, 2014, **16**, 5545

Aggregation induced blue-shifted emission – the molecular picture from a QM/MM study†

Qunyan Wu,‡[a] Tian Zhang,‡[a] Qian Peng,*[b] Dong Wang[a] and Zhigang Shuai*[a]

Received 20th November 2013,
Accepted 23rd January 2014

DOI: 10.1039/c3cp54910k

www.rsc.org/pccp

In general, optical emission in the solid-state is red-shifted with respect to the solution phase. A series of recently synthesized compounds exhibits aggregation induced blue-shifted emission (AIBSE) phenomena. By employing a polarizable continuum model (PCM) and a hybrid quantum mechanics/molecular mechanics (QM/MM) approach, we investigate the excited-state electronic structures of some typical AIE-active molecules both in solvents and in aggregates at the time-dependent density functional theory (TD-DFT) level. It is found that the AIBSE phenomena originate from the smaller reorganization energy in aggregates than in the solution phase, as evidenced through the restricted structural relaxation, planarization in the excited state, and freezing of low-frequency out-of-plane twists in the transition state.

1. Introduction

Efficient luminescent materials have attracted great attention due to their potential applications in solid-state display and lighting devices and bio-sensing. Most organic optoelectronic devices operate in the solid state.[1–4] It has been long known that molecular aggregates often cause both luminescence quenching and emission red-shift. There are several origins for the former: (i) intermolecular charge transfer which reduces the probability of electron–hole recombination; (ii) intermolecular excitation energy transfer eventually to the trap state; (iii) or formation of the low emissive 'side-by-side' H-aggregates with the dipole-forbidden nature of the emitting state[5] or detrimental species such as excimers with strong π–π interactions.[6,7] Gierschner and Park demonstrated recently that single crystals with H-aggregate packing can be highly emissive, in sharp contrast to the conventional wisdom.[8] The aggregation-induced red-shifted emission spectra could be ascribed to (i) excitonic coupling resulting from Coulombic interaction of spatial distribution of the transition dipole densities;[8] (ii) the anisotropic polarizability induced by the crystalline environment;[9,10] (iii) the charge-transfer (CT) character giving rise to a new intermolecular coordinate in the geometry change in π-stacks;[5] (iv) formation of J-aggregates;[5,11] (v) the smaller band gap arising from the increased band widths of both the HOMO- and the LUMO-derived bands according to a tight-binding model.[12] Thus, this is intriguing for compounds exhibiting aggregation induced blue-shifted emission (AIBSE) phenomena. The blue-shifted solid-state emission spectra were earlier observed in the substituted oligophenylenevinylene (**OPV**) microcrystals.[9,13] Then, they were found to be widely present in the solid-phase strong emitters with the so-called "aggregation-induced emission" (AIE) characteristic.[6,14–20] For example, the absorption band of 9,10-distyrylanthracene (**DSA**) in dilute THF solution peaks at 407 nm (3.05 eV), and the photoluminescence spectrum exhibits orange emission with a peak at 612 nm (2.03 eV).[15] While the absorption band of solid **DSA** particles in the THF/H_2O mixture (THF/H_2O = 1 : 3 v/v) is very similar to that in dilute THF solution, peaking at 414 nm (2.99 eV),[14] but the emission spectrum of the **DSA** crystal exhibits an obvious blue-shifted peak at 518 nm (2.39 eV).[15] The absorption and emission maxima of 2,3-dicyano-5,6-diphenylpyrazine (**DCDPP**) in dilute THF solution are 340 nm (3.65 eV) and 423 nm (2.93 eV), respectively.[16] When mixing a 90% volume fraction of water in THF, the absorption peak of **DCDPP** suspension in the THF–H_2O mixture remains unchanged, but the emission spectrum shows a blue-shifted peak at 413 nm (3.00 eV).[16] The absorption and emission maxima of *cis*,*cis*-1,2,3,4-tetraphenyl-1,3-butadiene (**TPBD**) in dilute acetone solution are 334 nm (3.71 eV) and 408 nm (3.04 eV), respectively.[17] When adding a 90% volume fraction of water to acetone, the absorption peak of **TPBD** aggregates in an acetone–H_2O mixture experiences a slight red shift peaking at 344 nm (3.60 eV), but the emission spectrum shows a blue-shifted peak at 390 nm (3.18 eV).[17]

The AIBSE phenomena are quite surprising experimental findings and the underlying mechanism is still unclear due to the difficulty in microscopic structural characterization. It was

[a] *Key Laboratory of Organic OptoElectronics and Molecular Engineering, Department of Chemistry, Tsinghua University, Beijing 100084, P. R. China. E-mail: zgshuai@tsinghua.edu.cn*
[b] *Key Laboratory of Organic Solids, Beijing National Laboratory for Molecular Science (BNLMS), Institute of Chemistry, Chinese Academy of Sciences, Beijing 100190, P. R. China. E-mail: qpeng@iccas.ac.cn*

† Electronic supplementary information (ESI) available: Supplementary figures and tables. See DOI: 10.1039/c3cp54910k

‡ These authors contributed equally.

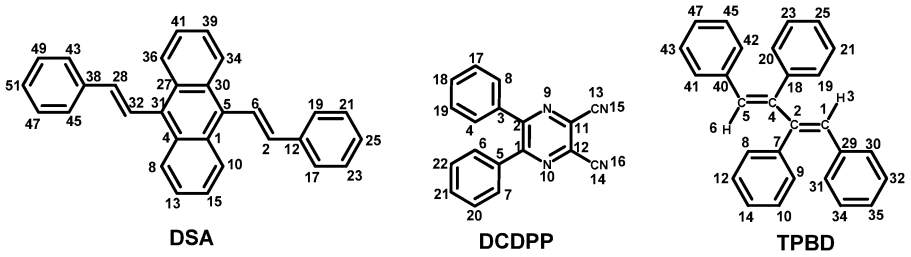

Chart 1 The chemical structures of **DSA**, **DCDPP**, and **TPBD**.

speculated that the twisted conformation in the solid state leads to less effective delocalization, which might be responsible for the blue shifts.[6,14] However, this would cause both blue-shifted absorption and emission. Another speculation is the formation of a twisted intramolecular charge transfer (TICT) state in the polar solvent and a locally excited state in aggregates due to restricted intramolecular rotation, which causes intensified and blue-shifted emission in the solid state.[21] However, this requires the molecule to contain strong donor and acceptor groups. In fact, this experimental observation shows that there is a slight red shift or hardly any shift in absorption, while the emission is remarkably blue-shifted. **DSA**, for example, when going from dilute tetrahydrofuran (THF) solution to the solid state, undergoes a slight red shift (7 nm, 0.06 eV) in its absorption maximum, but its emission maximum experiences a quite remarkable blue shift (94 nm, 0.36 eV) from 612 nm to 518 nm, with an approximately 100-fold increment in its fluorescence quantum yield.[14,15]

To better understand the mechanisms of such intriguing AIBSE phenomena, we have carried out theoretical and computational investigations for the excited-state structures both in dilute solution and in aggregates. Previously, the AIE phenomena have been theoretically explored by performing quantum mechanical/molecular mechanical (QM/MM) calculations, which provided a quantitative understanding.[22–24] In this contribution, we adopted the same computational approach to mimic the aggregation behaviors of **DSA**, **DCDPP**, and **TPBD** (Chart 1). Through carefully analyzing geometric and excited-state energetic properties of these molecules both in dilute solution and aggregates, we found that the blue-shifted emission is originated from the smaller reorganization energy in aggregates compared to the solution phase, which is induced by restricted geometric relaxation from $\mathbf{S_1}$ to $\mathbf{S_0}$, excited-state planarization and freezing of low-frequency out-of-plane vibrations.

2. Theoretical model and computational methodology

The basic model adopted in this work is the adiabatic potential-energy surface (PES) as shown in Chart 2, and Q refers to the nuclear configuration. $E_{\mathrm{em(ab)}}$ is the emission (absorption) energy, and $\lambda_{\mathrm{gs(es)}}$ is the reorganization energy of the ground state $\mathbf{S_0}$ (the first excited state $\mathbf{S_1}$). The total reorganization

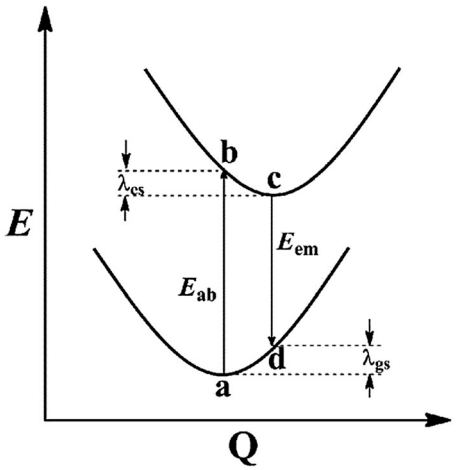

Chart 2 Schematic representation of the adiabatic potential energy surfaces (PES) for $\mathbf{S_0}$ and $\mathbf{S_1}$.

energy (λ), which corresponds to the Stokes shift observed in experiment, is expressed as the sum of λ_{gs} and λ_{es}. The emission energy can be expressed as the absorption energy minus the total reorganization energy:

$$E_{\mathrm{em}} = E_{\mathrm{ab}} - \lambda \quad (1)$$

When going from aggregate (aggr) to solution (sol), the shifted emission is obtained through simple subtraction:

$$\Delta E_{\mathrm{em}}^{\mathrm{aggr-sol}} = \Delta E_{\mathrm{ab}}^{\mathrm{aggr-sol}} + \lambda^{\mathrm{sol-aggr}} \quad (2)$$

We note that for strongly coupled excitons or excimer-like π–π interaction, in both absorption and emission, there should be $\Delta E^{\mathrm{aggr-sol}} < 0$, namely, the normal red shift. However, for some AIE-active molecules, usually with several twistable phenyl rings attached to the conjugated backbone of the chromophores, the intermolecular π–π stacking is often negligible due to the large intermolecular π–π interaction distance in crystals (Fig. S1–S3, ESI†), and the intramolecular motions dominate the photophysical processes.[22–24] In this case, the λ term could be much more pronounced in solution than that in aggregates, resulting in a large positive term $\lambda^{\mathrm{sol-aggr}}$ in eqn (2). Thus, the emission can exhibit a remarkable blue shift if the absorption shift is minor, whether red or blue. The blue-shifted emission implies $\Delta E_{\mathrm{em}}^{\mathrm{aggr-sol}} > 0$.

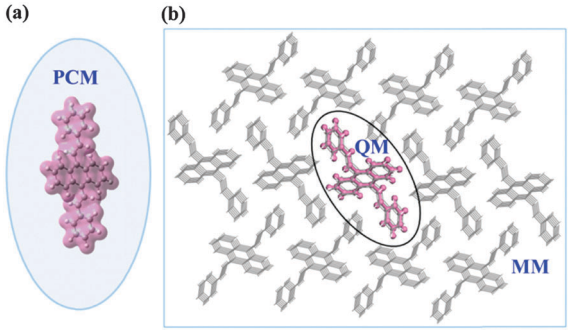

Chart 3 Setup of PCM (a) and QM/MM (b) models (taking **DSA** as an example).

We build our computational models as illustrated in Chart 3. We look at the molecular structures in both the ground state and the first excited state, in the solution phase and in the aggregate phase, respectively. The solvent effect is modeled using the polarizable continuum model (PCM).[25–27] The aggregate is modeled using an approach combining quantum mechanics and molecular mechanics (QM/MM),[28] where one electronically excited molecule is treated using the time-dependent density functional theory (TD-DFT), and the surrounding molecules are modeled using the general Amber force field (GAFF).[29] The aggregate structure is built by cutting a cluster from the crystal structure.[14,16,30]

All PCM calculations were performed using the D.01 version of Gaussian 09 package.[31] The absorption maximum has been determined under the non-equilibrium condition, equilibrating the reaction field with respect to the ground-state density, *i.e.*, state-specific non-equilibrium solvation. The vertical emission data are computed with the reaction field consistent with the emitting state, *i.e.*, state-specific equilibrium solvation. The solution-phase analytical $\mathbf{S_0}$ frequencies at the DFT level and numerical $\mathbf{S_1}$ frequencies at the TD-DFT level have been evaluated to check the absence of imaginary frequencies. The QM/MM was interfaced by using the ChemShell 3.5 package,[32] with the geometry optimized through the hybrid delocalized internal coordinate (HDLC) optimizer.[33] Turbomole 6.5[34,35] and DL-POLY[36] programs were used to calculate the energies and energy gradients of the QM and MM regions, respectively. The electrostatic embedding scheme with QM polarization was adopted.[37] Note that during the QM/MM geometry optimizations, only the QM molecule was active, and the surrounding molecules were kept frozen. The vibrational frequencies were obtained by using a numerical two-point displacement method and the electric polarization of the environment is included.

The structures and energies for the crucial points (a, b, c and d) in the adiabatic potential energy surface (PES) were determined at the level of DFT/TD-DFT. No symmetric constraint was adopted for the geometric optimization for both solution and aggregates. Grimme's D3-correction with Becke–Johnson damping [D3(bj)], was applied to include London-dispersion.[38–40] Optimizations and vibrational-frequency calculations for $\mathbf{S_0}$ and $\mathbf{S_1}$ were performed with PBE0[41] and B3LYP[42,43] functionals using the 6-31G* basis set. The PBE0 functional has been proved to be one of the most accurate estimates for describing the singlet-excited states of organic molecules from extensive TD-DFT benchmarks.[44–46] In the main text, we will discuss the geometric and energetic properties at the PBE0-D3(bj)/6-31G* level.

3. Results and discussion

3.1 Electronic structure and vertical transition energy

The local minima of $\mathbf{S_0}$ and $\mathbf{S_1}$ are determined by optimizing the geometries and calculating the normal-mode vibrational frequencies. The geometric parameters and energies at a, b, c and d points in the PES are determined both in solution and in aggregates (see Tables S1–S8, ESI†). TD-DFT calculations show that the $\mathbf{S_1}$ states of **DSA**, **DCDPP** and **TPBD** are all dominated by the transition from HOMO to LUMO in both solution and aggregate phases. The related oscillator strengths and assignments of $\mathbf{S_1}$ are also given (Tables S9–S10, ESI†). In order to better understand the electronic nature of the excited properties of these molecules, the electronic density contours of HOMOs and LUMOs are plotted (Fig. S4, ESI†). The vertical transition energies (E_{ab} and E_{em}), total reorganization energy (λ) and the adiabatic excitation energies (E_{ad}) are obtained according to Chart 2 (Table 1 and Tables S11–S16, ESI†). Vertical transition energies (relevant for absorption and emission peaks) for **DSA**, **DCDPP** and **TPBD** both in solution and aggregates are plotted in Fig. 1, together with the experimental values. Detailed comparisons between theoretical calculations at the TD-PBE0-D3(bj)/6-31G* level and the experimental observations are presented in Table 1.

It is noticed that for the three compounds: (i) both the predicted absorption maxima (vertical absorption energies) and emission maxima (vertical emission energies) are blue-shifted

Table 1 The electronic vertical transition energies corresponding to absorption and emission peaks for **DSA**, **DCDPP** and **TPBD** in both aggregate and solution phases at the TD-PBE0-D3(bj)/6-31G* level. The available experimental values are presented in the parentheses

	Absorption			Emission		
	ΔE_{ab}^{aggr}/eV	ΔE_{ab}^{solu}/eV	$\Delta E_{ab}^{aggr-solu}$/eV	ΔE_{em}^{aggr}/eV	ΔE_{em}^{solu}/eV	$\Delta E_{em}^{aggr-solu}$/eV
DSA	2.96 (2.99[a])	2.79 (3.05[b])	0.17 (−0.06)	2.32 (2.39[c])	2.05 (2.03[b])	0.27 (0.36)
DCDPP	3.49 (3.65[d])	3.34 (3.65[e])	0.15 (0.00)	2.66 (3.00[d])	2.29 (2.93[e])	0.37 (0.07)
TPBD	3.83 (3.60[f])	3.62 (3.71[g])	0.21 (−0.11)	3.09 (3.18[f])	2.58 (3.04[g])	0.51 (0.14)

[a] In the THF–water mixture (1 : 3 by volume). [b] In THF solution (~10 μM). [c] Crystal, from ref. 4. [d] In the THF–water mixture (1 : 9 by volume). [e] In THF solution (4 μM), from ref. 5. [f] In the acetone–water mixture (1 : 9 by volume). [g] In acetone solution (10 μM), from ref. 6.

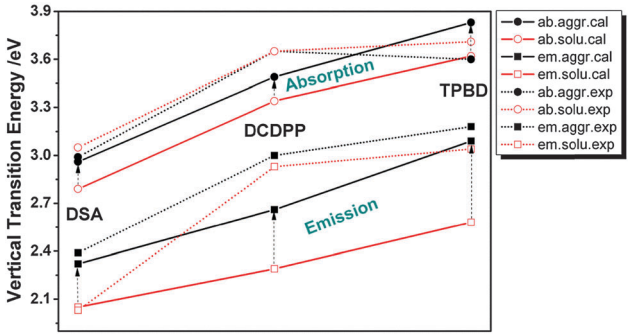

Fig. 1 Vertical transition energies corresponding to both absorption and emission peaks for **DSA**, **DCDPP** and **TPBD** at the PBE0-D3(bj)/6-31G* level. ● and ○ with connected solid [dotted] lines denote the calculated [experimental] vertical absorption energies (ab.) in aggregates (aggr.) and solution (solu.). ■ and □ with connected solid [dotted] lines denote the calculated [experimental] vertical emission energies (em.) in aggregates and solution.

from solution to aggregates; (ii) the magnitudes of the blue shifts in emission are much more pronounced than those in absorption. Namely, the Stokes shift measuring the difference between the absorption and emission maxima is strongly decreased from solution to aggregates. The former implies that the calculated blue-shifted absorption contributes a portion to the blue-shifted emission according to eqn (2), and could be ascribed to the effect of the crystal environment on the frontier molecular orbitals. The calculated HOMO–LUMO energy gaps at their $\mathbf{S_0}$ equilibrium geometry are all larger in aggregates than those in solution for the three molecules (Table 2), indicating that the intramolecular conjugation is diminished upon crystallization. For **DSA**, the dihedral angles between the 9,10-anthraylene core and the vinylene moiety (C27–C31–C32–C28 and C1–C5–C6–C2) of $\mathbf{S_0}$ are about 63° in aggregates, larger than those (53°) in solution. For **DCDPP**, the dihedral angles (C1–C2–C3–C4 and C2–C1–C5–C6) of $\mathbf{S_0}$ are about 45° in aggregates, while the corresponding values are about 38° in solution. For **TPBD**, two mid-phenyls (C5–C4–C18–C20 and C1–C2–C7–C9) of $\mathbf{S_0}$ are about 69° in aggregates and 64° in solution; two side-phenyls (C4–C5–C40–C42 and C2–C1–C29–C31) of $\mathbf{S_0}$ are approximately 33° in aggregates and 26° in solution. In other words, the twisted peripheral phenyl rings

Table 2 HOMO and LUMO energies, HOMO–LUMO gaps (eV) at the $\mathbf{S_0}$ equilibrium geometry for **DSA**, **DCDPP** and **TPBD** at the PBE0-D3(bj)/6-31G* and B3LYP-D3(bj)/6-31G* levels for aggregates (QM/MM) and solution (PCM)

		Aggregate			Solution		
	Functional	HOMO	LUMO	ΔE_{H-L}	HOMO	LUMO	ΔE_{H-L}
DSA	PBE0-D3(bj)	−4.92	−1.41	3.51	−5.28	−1.99	3.29
	B3LYP-D3(bj)	−4.58	−1.37	3.21	−5.01	−2.02	2.99
DCDPP	PBE0-D3(bj)	−7.23	−3.03	4.20	−6.88	−2.72	4.16
	B3LYP-D3(bj)	−6.85	−3.02	3.83	−6.58	−2.78	3.80
TPBD	PBE0-D3(bj)	−5.24	−1.00	4.24	−5.61	−1.59	4.02
	B3LYP-D3(bj)	−4.90	−1.00	3.90	−5.33	−1.64	3.69

or vinylene moieties help the central planar chromophore struggle to form excimers in aggregates, leading to less effective π conjugation. The latter embodies the important role of the λ term in eqn (2). A large positive term $\lambda^{sol-aggr}$ leads to the remarkable blue-shifted emission found in experiment. It is also possible that blue-shifted emission would occur even when there is no shift or a slight red shift in absorption according to eqn (2). It is noticed that for **DSA**, the calculated blue-shifted value (0.27 eV) is quite similar to that in experiment (0.36 eV), and the experimental solid-phase reference is a crystal; while for **DCDPP** and **TPBD**, the available experimental results are for amorphous nanoparticles. It has also been reported that many AIE-active dyes emit blue-shifted lights with higher efficiencies in the crystalline phase than in the amorphous phase.[47–49] Our calculations are performed with crystal structure, and therefore for DCDPP and TPBD, the calculated results correlated less well than for DSA. Also, the vertical emission energies are underestimated for **DCDPP** and **TPBD** in solution. To fully address this issue, an explicit QM/MM model together with a classic dynamic sampling[50] deserves future investigation. In our QM/MM model for the treatment of aggregates, we completely neglect the excitonic couplings and charge transfer effects, both could account for the slight red-shift in absorption. Indeed, fluorescence of molecular solids is a rather complicated problem, where both intramolecular (electronic oscillators and vibronic coupling) and intermolecular interactions (exciton diffusion, intermolecular arrangement, long-range order and chemical contamination)[8,9] come into play. In this work, we simply emphasize only one aspect that the blue-shifted emission is induced by intramolecular relaxation, which we believe is essential for such a class of molecules.

3.2 Rationalization of smaller Stokes shift in aggregates

Stokes' shift is in essence the total reorganization energy during the reciprocal transformation of two electronic states, which can be divided into λ_{gs} and λ_{es}. For clarity, we presented these quantities in Fig. 2. It can be seen that the total reorganization energy is much smaller in aggregates than that in

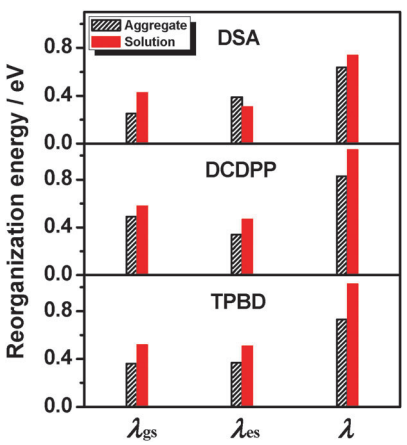

Fig. 2 Total reorganization energy ($\lambda = \lambda_{gs} + \lambda_{es}$) for **DSA**, **DCDPP** and **TPBD** in aggregate and solution at the PBE0-D3(bj)/6-31G* level.

solution. The two components (λ_{gs} and λ_{es}) also follow the same tendency except the counter-intuitive λ_{es} part of **DSA**. This may be ascribed to the "zigzag motif" as shown in Chart 3.[14] The peripheral rings nearly perpendicular to the anthracene skeleton have enough space to rotate in aggregates. However, this does not affect the change in the tendency of the total reorganization energy from solution to aggregates. We turn next to the discussion of geometric relaxation from S_1 to S_0, excited-state configurations and low-frequency out-of-plane vibrations.

3.2.1 Restricted geometric modification. The reorganization energy reflects the geometric relaxation in the molecule when going from S_0 to S_1, and *vice versa*. Smaller reorganization energies imply smaller structural changes in aggregates during the excited-state relaxation process. Optimized geometric parameters for these molecules in S_0, S_1 and the structural differences $|\Delta(S_0-S_1)|$ are listed, together with the X-ray crystal structure for comparison (Tables S1–S6, ESI†). The predicted structural parameters of S_0 are in excellent agreement with the crystal structure, which rationalize our QM/MM method. Selected torsion angles with major geometric modifications between S_0 and S_1 are shown in Fig. 3. It can be seen that: (i) for **DSA**, a torsion angle between the 9,10-anthrylene core and the vinylene moiety (C27–C31–C32–C28) and the central anthracene ring (C31–C4–C1–C5) tends to show a much smaller modification in aggregates from S_0 to S_1, but the peripheral rings (C32–C28–C38–C45) demonstrate the opposite trend. This is reminiscent of the counter-intuitive λ_{es} part of **DSA**. The electronic density of **DSA** is mainly distributed on the central anthracene ring and the neighboring double bonds and therefore the change in the relatively flexible vinylene moiety together with the central anthracene ring dominates the transition process. (ii) For **DCDPP**, all rotatable rings are restricted in aggregates and show smaller structural differences upon excitation. (iii) For **TPBD**, rotation of the main conjugated butadiene core (C1–C2–C4–C5) together with mid-phenyls (C1–C2–C7–C9) is obviously hindered although two side-phenyls (C2–C1–C29–C31) seem to be slightly active in aggregates. Indeed, the restricted intramolecular motion in aggregates echoes the smaller reorganization energy, and thus causes blue-shifted emission.

3.2.2 Excited-state planarization. For photoluminescence (PL) spectra in solution, Stokes shift is expected to be smaller if the chromophore shows planar configuration in the excited state.[51] This was discussed based on broad experimental evidence.[13] Quantum-chemical calculations support such correlation between the excited-state planarization and reduced reorganization energies in solution by studying per-fluorination of *para*-oligophenylenes and anilido-pyridine boron difluoride dyes.[52,53] To assess the influence of excited-state planarization, we list the corresponding structural parameters at their S_0 and S_1 equilibrium geometries (see Tables S1–S6, ESI†). It is seen that (i) for **DSA**, the dihedral angles (C31–C4–C1–C5 and C8–C4–C1–C10) related to the central anthracene ring at the S_1 equilibrium geometry are about 5° in aggregates, smaller than those (about 10°) in solution, indicating a relatively planar emitting state formed by the anthracene skeleton in aggregates; (ii) for **DCDPP**,

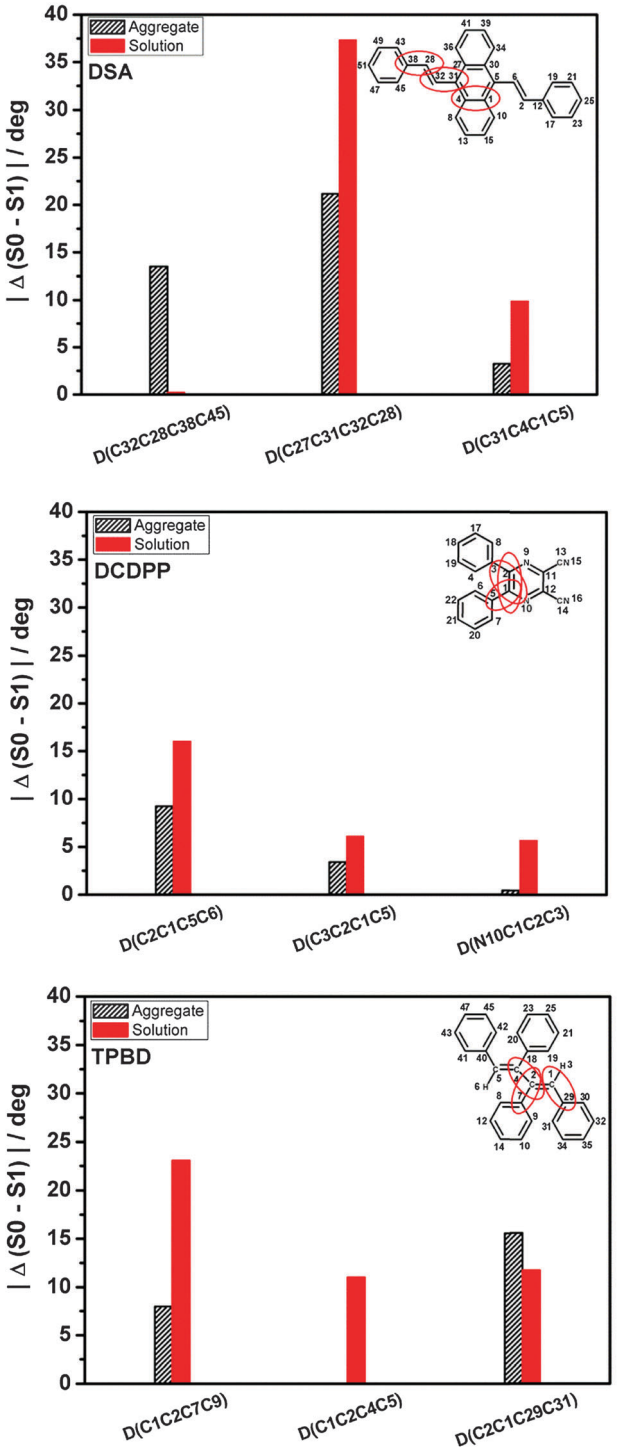

Fig. 3 Selected torsion angles with major geometric modifications between S_0 and S_1 for **DSA**, **DCDPP** and **TPBD** in aggregate and solution at the PBE0-D3(bj)/6-31G* level.

the dihedral angles (C11–N9–C2–C3, N10–C1–C2–C3 and C3–C2–C1–C5) of S_1 are about 175°, 175° and 11° in aggregates, respectively. However, the corresponding values are about 169°, 161°, and 21° in solution. This feature also indicates a more planar pyrazine ring in the solid phase; (iii) for **TPBD**, the dihedral angle (C1–C2–C4–C5) at the S_1 equilibrium geometry is 180° in

aggregates and about 154° in solution, implying a complete planarity of the butadiene core upon aggregation. In other words, excited-state planarization of the central choromophore in aggregates promotes the restricted geometric relaxation, and thus leads to the blue-shifted emission.

3.2.3 Freezing of low-frequency out-of-plane vibrations. In the displaced harmonic oscillator model, the Huang–Rhys (HR) factors directly connect with the displacement (D_i) along the normal mode i between the minima of the $\mathbf{S_0}$ and $\mathbf{S_1}$ equilibrium geometries and characterize the extent of geometric relaxation. The HR factors, $HR_i = (\omega_i D_i^2)/2\hbar$, are obtained through the DUSHIN program.[54] For **DCDPP**, it has been systematically investigated in our previous work that three modes with large HR factors all fall in the low-frequency region (<200 cm^{-1}), which are mainly assigned to out-of-plane twisting motions of the phenyl rings.[55] These torsional modes contribute largely to the reorganization energies and result in the large Stokes shift in the gas or solution phase. However, such torsional motions are hindered in aggregates, and the HR factors together with the reorganization energies of the three modes become much smaller, leading to the reduced Stokes shift.[23,55] For **DSA** and **TPBD**, the large HR factors ($HR_i > 1$) *versus* the normal mode at $\mathbf{S_0}$ in both aggregates and solution are listed in Table 3. It is seen that (i) there are more vibration modes with large HR factors in solution than in aggregates; (ii) most of these modes display a remarkable decrease in HR factors from solution to aggregates, which demonstrates a strong geometric distortion upon excitation in solution; (iii) the diagrammatic illustrations of the selected normal modes in solution with evidently decreased HR factors from solution to aggregates are depicted (Fig. S5, ESI†). These coordinates related to the out-of-plane motions are associated with a large Stokes shift, much larger than that of other coordinates, such as C–C or C–H stretching. Consequently, these molecules show an emission at significantly longer wavelengths in solution. When these molecules are in a rigid matrix or in crystal form, such low-frequency out-of-plane motions are inhibited. Therefore, AIBSE is an obvious consequence of the aggregation-induced freezing of low-frequency out-of-plane vibrations and of the consequent change in their Franck–Condon factors.

Table 3 Selected normal modes with Huang–Rhys factors ($HR_i > 1$) in aggregates and in solution, as well as harmonic vibrational frequencies (ω_i) of $\mathbf{S_0}$ for **DSA** and **TPBD**

Aggregate			Solution		
Mode i	ω_i/cm^{-1}	HR_i	Mode i	ω_i/cm^{-1}	HR_i
DSA					
3	91	2.07	2	12	3.74
8	158	2.69	3	14	35.98
11	173	6.06	4	25	2.00
17	320	1.74	7	74	3.55
			9	105	10.44
			13	159	1.17
			16	255	1.30
TPBD					
8	134	2.21	2	22	12.21
			4	39	5.61
			12	178	1.18

3.3 Robustness of the computational reorganization energy – the effects of ZPE, functionals and basis sets

Now we will discuss the robustness of the computational results. Zero-point vibrational energy (ZPE) correction, choices of functionals, as well as basis-set completeness can certainly affect the computational results. Once considering the ZPE contribution, both the absorption and emission maxima with respect to the vertical transition energies from the minima of parabola are red-shifted by approximately 0.03–0.14 eV. Nevertheless, the magnitudes of the red shifts are the same in both absorption and emission, and the ZPE corrected $\Delta E_{em}^{aggr-solu}$ is still much larger than the ZPE corrected $\Delta E_{em}^{aggr-solu}$ for **DSA**, **DCDPP** and **TPBD** (Table 1 and Table S11, ESI†). The reorganization energies remain unchanged because the ZPE at the a (b) point is the same as that at the d (c) point in the PES (Table S12, ESI†). Choices of functionals are now ample. We find that B3LYP-D3(bj) gives nearly the same geometric modification tendency between $\mathbf{S_0}$ and $\mathbf{S_1}$ as the PBE0-D3(bj) functional (Tables S1–S6, ESI†). The vertical transition energies and the reorganization energies of **DSA**, **DCDPP** and **TPBD** are also quite similar to results at the PBE0-D3(bj)/6-31G* level (Tables S13–S15, ESI†). TD-DFT generally offers rapid yet accurate estimations for the electronic transition energies.[56,57] The TD-DFT charge-transfer issue is particularly problematic.[58] The recently developed long-range corrected functionals, such as CAM-B3LYP,[59] have shown promise in resolving the charge-transfer deficiencies of TD-DFT.[60] We then recalculated the vertical transition energy and the reorganization energies using the CAM-B3LYP-D3(bj) functional based on the structure determined at the (TD)-PBE0-D3(bj)/6-31G* level. The single-point vertical excitation-energy calculations were carried out by adding charges to the QM part using Gaussian 09 program. The added charges mimic the surrounding MM parts obtained by the above QM/MM optimizations. The vertical transition energies for the three molecules with the long-range corrected CAM-B3LYP-D3(bj) functional are blue-shifted by about 0.13–0.54 eV in comparison with those obtained by using the PBE0-D3(bj) functional, also in agreement with experimental results (Table S17, ESI†). And most importantly, the pronounced positive $\lambda^{solu-aggr}$ nature is unchanged (Table S18, ESI†).

Basis-set incompleteness errors (BSIE) were noticed and should be benchmarked. To reduce the computational efforts, single-point vertical excitation-energy calculations were carried out based on the stable structures determined at the (TD)-PBE0-D3(bj)/6-31G* level. We have evaluated the dependence of larger TZVP with triple-ζ quality and 6-31 + G* with a diffuse function on the vertical transition energies and reorganization energies. It was found that when going from double-ζ 6-31G* to triple-ζ TZVP, the vertical transition energies were decreased by about 0.02–0.09 eV (Table S19, ESI†). Addition of diffuse functions to second-row elements in the periodic table gives the same magnitudes of red shifts (Table S20, ESI†). Even so, the

values of $\lambda^{solu-aggr}$ terms are almost the same as the small 6-31G* basis set (Tables S21–S22, ESI†).

Thus, through extensive computations, we find the effects of ZPE, functionals and basis sets do not change the quantitative conclusions.

4. Conclusion

To summarize, we have presented a multiscale quantum chemistry investigation on the exotic AIBSE phenomenon, *i.e.*, the absorption is relatively unaffected but the emission undergoes a remarkable blue shift from solution to aggregates, taking **DSA**, **DCDPP** and **TPBD** as examples, in sharp contrast to the conventional solid-state red-shifted emitting behavior. We point out that this primarily originates from the smaller reorganization energy in aggregates compared to the solution, as induced by a restricted geometric change, excited-state planarization and freezing of low-frequency out-of-plane vibrations during the excited-state relaxation. Through computational chemistry, we justify this assumption by determining the structures and energies for the crucial points (a, b, c and d) in the PES taking both solvent effect and aggregation environment into account, using PCM and QM/MM approaches, respectively. The theoretical results give support to the existing experimental findings and reveal the nature of the AIBSE phenomena. In fact, from this study, we conclude that such blue shift is universal if the AIE mechanism is indeed the restricted intramolecular rotation (RIR). Namely, aggregation tends to suppress the non-radiative decay process through intermolecular hindrance, while leaving radiative decay dominant. The AIBSE is another outcome of such an effect.

In the present method, the following approximations are made: (i) we assumed that the intermolecular interactions are weak and there are no appreciable intermolecular charge or energy transfers or excitonic effects between neighboring molecules; (ii) MM polarization by the electron-density change of the QM molecule in the excited state was not taken into account due to the limitation of GAFF. Conventional molecular exciton theory usually takes one or two vibrational modes with fixed exciton–vibration coupling (Huang–Rhys factor). Nevertheless, in this work, we shine light on the molecular picture mentioned above, induced by restricted intramolecular motion in aggregates, which leads to the blue-shifted emission. So far, the excitonic model often ignored this molecular feature. This work cautions the application of such treatment and calls for excitonic theory with consideration of intramolecular relaxation.[61]

Acknowledgements

TZ is deeply indebted to Dr Likai Du for the help with the QM/MM method and Dr Peng Cui concerning the computational codes. The authors thank Profs Junwu Chen and Wenjing Tian, and Dr Bin Xu for extensive discussions on their experimental findings. This work is supported by the National Natural Science Foundation of China (Grant No. 21290190, 21103097, 21121004, and 91233105), and the Ministry of Science and Technology of China through 973 program (Grant No. 2013CB834703, 2013CB933503, and 2011CB808400).

References

1 J. A. Rogers, T. Someya and Y. G. Huang, *Science*, 2010, **327**, 1543–1678.
2 R. D. Miller and E. A. Chandross, *Chem. Rev.*, 2010, **110**, 1–574.
3 W. Z. Yuan, P. Lu, S. M. Chen, J. W. Y. Lam, Z. M. Wang, Y. Liu, H. S. Kwok, Y. G. Ma and B. Z. Tang, *Adv. Mater.*, 2010, **22**, 2159–2163.
4 W. Z. Yuan, Y. Q. Tan, Y. Y. Gong, P. Lu, J. W. Y. Lam, X. Y. Shen, C. F. Feng, H. H. Y. Sung, Y. W. Lu, I. D. Williams, J. Z. Sun, Y. M. Zhang and B. Z. Tang, *Adv. Mater.*, 2013, **25**, 2837–2843.
5 J. Gierschner, L. Lüer, B. Milián-Medina, D. Oelkrug and H.-J. Egelhaaf, *J. Phys. Chem. Lett.*, 2013, **4**, 2686–2697.
6 Y. N. Hong, J. W. Y. Lam and B. Z. Tang, *Chem. Commun.*, 2009, 4332–4353.
7 Y. N. Hong, J. W. Y. Lam and B. Z. Tang, *Chem. Soc. Rev.*, 2011, **40**, 5361–5388.
8 J. Gierschner and S. Y. Park, *J. Mater. Chem. C*, 2013, **1**, 5818–5832.
9 D. Oelkrug, A. Tompert, H.-J. Egelhaaf, M. Hanack, E. Steinhuber, M. Hohloch, H. Meier and U. Stalmach, *Synth. Met.*, 1996, **83**, 231–237.
10 Y.-S. Huang, J. Gierschner, J. P. Schmidtke, R. H. Friend and D. Beljonne, *Phys. Rev. B: Condens. Matter Mater. Phys.*, 2011, **84**, 205311.
11 B.-K. An, S.-K. Kwon, S.-D. Jung and S. Y. Park, *J. Am. Chem. Soc.*, 2002, **124**, 14410–14415.
12 Y. J. Dong, B. Xu, J. B. Zhang, X. Tan, L. J. Wang, J. L. Chen, H. G. Lv, S. P. Wen, B. Li, L. Ye, B. Zou and W. J. Tian, *Angew. Chem., Int. Ed.*, 2012, **51**, 10782–10785.
13 D. Oelkrug, A. Tompert, J. Gierschner, H.-J. Egelhaaf, M. Hanack, M. Hohloch and E. Steinhuber, *J. Phys. Chem. B*, 1998, **102**, 1902–1907.
14 J. T. He, B. Xu, F. P. Chen, H. J. Xia, K. P. Li, L. Ye and W. J. Tian, *J. Phys. Chem. C*, 2009, **113**, 9892–9899.
15 Y. J. Dong, B. Xu, J. B. Zhang, H. G. Lu, S. P. Wen, F. P. Chen, J. T. He, B. Li, L. Ye and W. J. Tian, *CrystEngComm*, 2012, **14**, 6593–6598.
16 A. J. Qin, J. W. Y. Lam, F. Mahtab, C. K. W. Jim, L. Tang, J. Z. Sun, H. H. Y. Sung, I. D. Williams and B. Z. Tang, *Appl. Phys. Lett.*, 2009, **94**, 253308.
17 J. W. Chen, B. Xu, X. Y. Ouyang, B. Z. Tang and Y. Cao, *J. Phys. Chem. A*, 2004, **108**, 7522–7526.
18 Z. Li, Y. Q. Dong, B. X. Mi, Y. H. Tang, M. Häussler, H. Tong, Y. P. Dong, J. W. Y. Lam, Y. Ren, H. H. Y. Sung, K. S. Wong, P. Gao, I. D. Williams, H. S. Kwok and B. Z. Tang, *J. Phys. Chem. B*, 2005, **109**, 10061–10066.
19 K. A. N. Upamali, L. A. Estrada, P. K. De, X. C. Cai, J. A. Krause and D. C. Neckers, *Langmuir*, 2011, **27**, 1573–1580.

20 X. Y. Shen, Y. J. Wang, E. G. Zhao, W. Z. Yuan, Y. Liu, P. Lu, A. J. Qin, Y. G. Ma, J. Z. Sun and B. Z. Tang, *J. Phys. Chem. C*, 2013, **117**, 7334–7347.
21 R. R. Hu, E. Lager, A. l. Aguilar-Aguilar, J. Z. Liu, J. W. Y. Lam, H. H. Y. Sung, I. D. Williams, Y. C. Zhong, K. S. Wong, E. Peña-Cabrera and B. Z. Tang, *J. Phys. Chem. C*, 2009, **113**, 15845–15853.
22 M.-C. Li, M. Hayashi and S.-H. Lin, *J. Phys. Chem. A*, 2011, **115**, 14531–14538.
23 Q. Y. Wu, C. M. Deng, Q. Peng, Y. L. Niu and Z. G. Shuai, *J. Comput. Chem.*, 2012, **33**, 1862–1869.
24 Q. Y. Wu, Q. Peng, Y. L. Niu, X. Gao and Z. G. Shuai, *J. Phys. Chem. A*, 2012, **116**, 3881–3888.
25 M. Cossi and V. Barone, *J. Chem. Phys.*, 2001, **115**, 4708–4717.
26 G. Scalmani, M. J. Frisch, B. Mennucci, J. Tomasi, R. Cammi and V. Barone, *J. Chem. Phys.*, 2006, **124**, 094107.
27 R. Improta, V. Barone, G. Scalmani and M. J. Frisch, *J. Chem. Phys.*, 2006, **125**, 054103.
28 A. Warshel and M. Levitt, *J. Mol. Biol.*, 1976, **103**, 227–249.
29 J. M. Wang, R. M. Wolf, J. W. Caldwell, P. A. Kollman and D. A. Case, *J. Comput. Chem.*, 2004, **25**, 1157–1174.
30 I. L. Karle and K. S. Dragonette, *Acta Crystallogr.*, 1965, **19**, 500–503.
31 M. J. Frisch, G. W. Trucks, H. B. Schlegel, G. E. Scuseria, M. A. Robb, J. R. Cheeseman, G. Scalmani, V. Barone, B. Mennucci, G. A. Petersson, H. Nakatsuji, M. Caricato, X. Li, H. P. Hratchian, A. F. Izmaylov, J. Bloino, G. Zheng, J. L. Sonnenberg, M. Hada, M. Ehara, K. Toyota, R. Fukuda, J. Hasegawa, M. Ishida, T. Nakajima, Y. Honda, O. Kitao, H. Nakai, T. Vreven, J. A. Montgomery Jr, J. E. Peralta, F. Ogliaro, M. Bearpark, J. J. Heyd, E. Brothers, K. N. Kudin, V. N. Staroverov, R. Kobayashi, J. Normand, K. Raghavachari, A. Rendell, J. C. Burant, S. S. Iyengar, J. Tomasi, M. Cossi, N. Rega, J. M. Millam, M. Klene, J. E. Knox, J. B. Cross, V. Bakken, C. Adamo, J. Jaramillo, R. Gomperts, R. E. Stratmann, O. Yazyev, A. J. Austin, R. Cammi, C. Pomelli, J. W. Ochterski, R. L. Martin, K. Morokuma, V. G. Zakrzewski, G. A. Voth, P. Salvador, J. J. Dannenberg, S. Dapprich, A. D. Daniels, Ö. Farkas, J. B. Foresman, J. V. Ortiz, J. Cioslowski and D. J. Fox, *Gaussian 09, Revision D.01*, Gaussian Inc., Wallingford CT, 2013.
32 P. Sherwood, A. H. de Vries, M. F. Guest, G. Schreckenbach, C. R. A. Catlow, S. A. French, A. A. Sokol, S. T. Bromley, W. Thiel, A. J. Turner, S. Billeter, F. Terstegen, S. Thiel, J. Kendrick, S. C. Rogers, J. Casci, M. Watson, F. King, E. Karlsen, M. Sjøvoll, A. Fahmi, A. Schäfer and C. Lennartz, *THEOCHEM*, 2003, **632**, 1–28.
33 S. R. Billeter, A. J. Turner and W. Thiel, *Phys. Chem. Chem. Phys.*, 2000, **2**, 2177–2186.
34 TURBOMOLE V6.5 2013, University of Karlsruhe and of the Forschungszentrum Karlsruhe GmbH, 1989–2007; TURBOMOLE GmbH, since 2007 (accessed May 23, 2013).
35 R. Ahlrichs, M. Bär, M. Häser, H. Horn and C. KÖlmel, *Chem. Phys. Lett.*, 1989, **162**, 165–169.
36 W. Smith and T. R. Forester, *J. Mol. Graphics*, 1996, **14**, 136–141.
37 D. Bakowies and W. Thiel, *J. Phys. Chem.*, 1996, **100**, 10580–10594.
38 S. Grimme, J. Antony, S. Ehrlich and H. Krieg, *J. Chem. Phys.*, 2010, **132**, 154104.
39 S. Grimme, S. Ehrlich and L. Goerigk, *J. Comput. Chem.*, 2011, **32**, 1456–1465.
40 L. Goerigk and J. R. Reimers, *J. Chem. Theory Comput.*, 2013, **9**, 3240–3251.
41 C. Adamo and V. Barone, *J. Chem. Phys.*, 1999, **110**, 6158–6170.
42 A. D. Becke, *J. Chem. Phys.*, 1993, **98**, 5648–5652.
43 C. Lee, W. T. Yang and R. G. Parr, *Phys. Rev. B: Condens. Matter Mater. Phys.*, 1988, **37**, 785–789.
44 D. Jacquemin, E. A. Perpète, I. Ciofini and C. Adamo, *Acc. Chem. Res.*, 2009, **42**, 326–334.
45 D. Jacquemin, V. Wathelet, E. A. Perpète and C. Adamo, *J. Chem. Theory Comput.*, 2009, **5**, 2420–2435.
46 D. Jacquemin, A. Planchat, C. Adamo and B. Mennucci, *J. Chem. Theory Comput.*, 2012, **8**, 2359–2372.
47 J. W. Chen, B. Xu, K. X. Yang, Y. Cao, H. H. Y. Sung, I. D. Williams and B. Z. Tang, *J. Phys. Chem. B*, 2005, **109**, 17086–17093.
48 Y. Q. Dong, J. W. Y. Lam, A. J. Qin, Z. Li, J. Z. Sun, H. H. Y. Sung, I. D. Williams and B. Z. Tang, *Chem. Commun.*, 2007, 40–42.
49 H. Tong, Y. Dong, Y. Hong, M. Häussler, J. W. Y. Lam, H. H. Y. Sung, X. Yu, J. Sun, I. D. Williams, H. S. Kwok and B. Z. Tang, *J. Phys. Chem. C*, 2007, **111**, 2287–2294.
50 N. De Mitri, S. Monti, G. Prampolini and V. Barone, *J. Chem. Theory Comput.*, 2013, **9**, 4507–4516.
51 I. B. Berlman, *J. Phys. Chem.*, 1970, **74**, 3085–3093.
52 B. Milián-Medina, S. Varghese, R. Ragni, H. Boerner, E. Ortí, G. M. Farinola and J. Gierschner, *J. Chem. Phys.*, 2011, **135**, 124509.
53 J.-L. Jin, H.-B. Li, Y. Geng, Y. Wu, Y.-A. Duan and Z.-M. Su, *ChemPhysChem*, 2012, **13**, 3714–3722.
54 J. R. Reimers, *J. Chem. Phys.*, 2001, **115**, 9103–9109.
55 C. M. Deng, Y. L. Niu, Q. Peng, A. J. Qin, Z. G. Shuai and B. Z. Tang, *J. Chem. Phys.*, 2011, **135**, 014304.
56 D. Jacquemin, E. A. Perpète, G. Scalmani, M. J. Frisch, I. Ciofini and C. Adamo, *Chem. Phys. Lett.*, 2007, **448**, 3–6.
57 D. Jacquemin, E. A. Perpète, G. Scalmani, I. Ciofini, C. Peltier and C. Adamo, *Chem. Phys.*, 2010, **372**, 61–66.
58 A. Lange and J. M. Herbert, *J. Chem. Theory Comput.*, 2007, **3**, 1680–1690.
59 T. Yanai, D. P. Tew and N. C. Handy, *Chem. Phys. Lett.*, 2004, **393**, 51–57.
60 M. A. Rohrdanz, K. M. Martins and J. M. Herbert, *J. Chem. Phys.*, 2009, **130**, 054112.
61 Z. G. Shuai, W. J. Liu, W. Z. Liang, Q. Shi and H. Chen, *Sci. China: Chem.*, 2013, **9**, 1258–1262.

